Mechanism of Controlled Release of Vancomycin from Crumpled Graphene Oxides

Xing He,*,[†,‖] Ziyan Zhou,[†,‖] Zhuo Han,[‡] Yang Zeng,[†] Xiaojie Chen,[†] and Jiacan Su*,[§]

[†]School of Material Science and Engineering, University of Shanghai for Science and Technology, 516 Jungong Road, Shanghai 200093, China

[‡]Department of Mechanical Engineering, Hong Kong Polytechnic University, Hung Hom, Kowloon 999077, Hong Kong, China

[§]Department of Orthopaedics Trauma, Changhai Hospital, Second Military Medical University, Shanghai 200433, China

ABSTRACT: The physical and chemical interactions with vancomycin (VAN) were accessed between graphene oxide (GO) and crumpled graphene oxide (CGO) to present the possible loading and release mechanisms. The improved hydrophilicity and surface charge were found on CGO through water contact angle and ζ-potential measurements. Fourier transform infrared and X-ray photoelectron spectroscopies confirmed the attachment of VAN onto CGO or GO through $\pi-\pi$ stacking and hydrogen bonding. Both CGO−VAN and GO−VAN drug complexes showed pH-controlled release property. The high VAN loading and delayed release in CGO−VAN system were mainly due to the crumpled morphology.
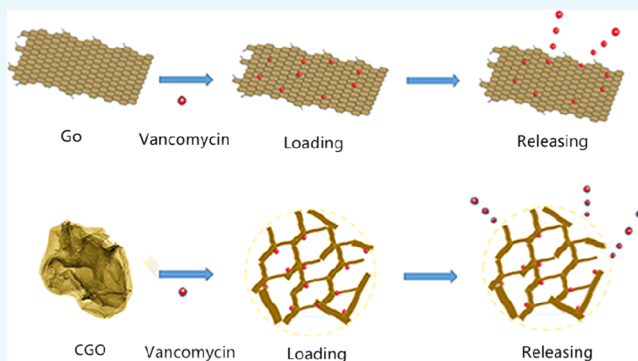
INTRODUCTION

Vancomycin was a branched tricyclic glycopeptide antibiotic with a molecular weight of 1450 Da and was frequently functioned as the inhibitor of bacterial cell wall synthesis through hydrogen bonds with peptidoglycan biopolymers.[1,2] Specifically, vancomycin was used to treat osteomyelitis,[3] pneumonitis,[4] sepsis,[5] and other bacterial infections, which were mainly caused by Gram-positive bacteria.[6] Because the large molecular size of vancomycin led to low penetration into poorly vascularized sites and its high concentration in blood increased the risk of nephrotoxicity,[7,8] the high local concentration of vancomycin was advantageous over intravenous injection for deep-seated infections such as bones and prosthetic devices. Delivering vancomycin using carrier materials was a promising strategy to prolong the residence time and improve the accumulation at the target infection site.[9,10] Various drug carrier materials, such as polymers,[11] liposomes,[12] mesoporous silica,[13] and other nanoparticles,[14] were developed to achieve sustainable local antibiotic administration. However, the instability in the physiological environment and low drug-loading efficiency restricted their applications.

Graphene derivatives were favorable drug carriers for high surface area of adsorption, and the release behavior could be modified by covalent or noncovalent bonding.[15,16] The reduced graphene oxides decorated by vancomycin were applied to heal wound infection caused by *Staphylococcus aureus* in a rat infection model.[17] Our early work involved three-dimensional (3D) graphene/hydroxyapatite scaffold, where the control of infection and regeneration of bone due

to the controlled release of vancomycin were demonstrated.[18] Graphene derivatives containing vancomycin could be effective carrier materials. Unlike other carrier materials,[19] their loading efficiencies were not fully investigated. At the same time, other important properties of graphene derivatives, such as lateral size[20] and morphology,[21] could also influence loading and release behaviors of vancomycin. Crumpled graphene oxide possessed spherical structures with ridges and wrinkles and was a candidate for drug carrier systems.[22] The application of crumpled graphene oxides for drug carrier was in its early stage, and no research had been undertaken on vancomycin to date.

Herein, the interaction with vancomycin molecules was accessed between graphene oxide and crumpled graphene oxide to highlight the high drug loading and pH-sensitive release. The results were based on the detailed discussion of microstructural and physicochemical characterizations of two graphene carriers.
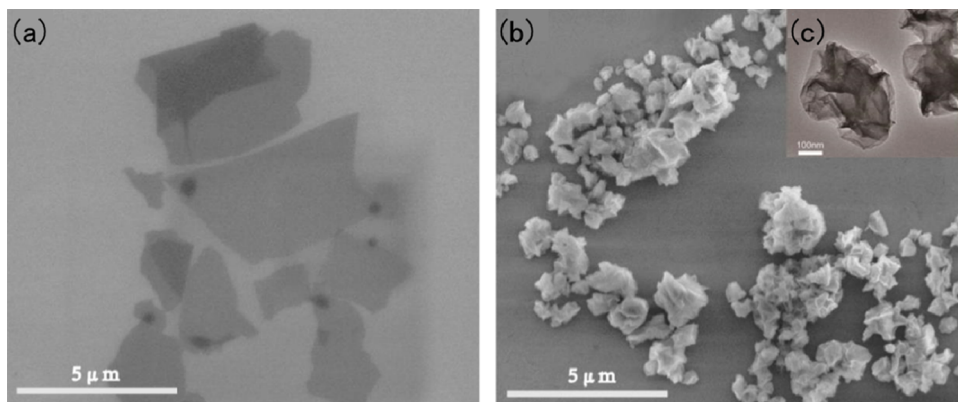
RESULTS AND DISCUSSION

Characterization of GO, CGO, GO−VAN, CGO−VAN Systems. The difference in morphology was distinguished between graphene oxides (GOs) and crumpled graphene oxides (CGOs). GO, which was obtained through oxidation and exfoliation of graphite in agitated solutions, was exhibited as a two-dimensional lamellar structure with micrometer-sized

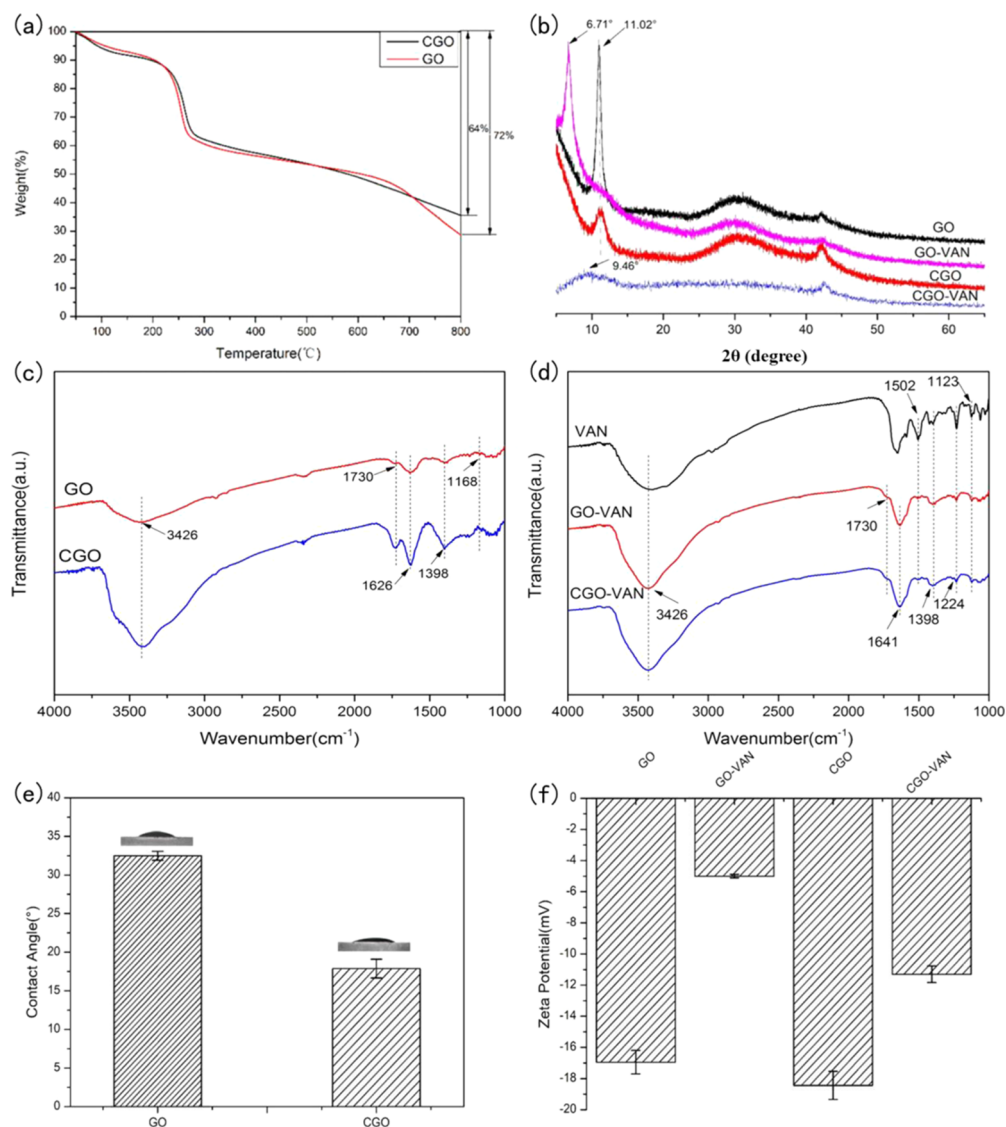**Figure 1.** SEM overviews of (a) micrometer-sized flat sheets of GO and (b) submicron-sized crumpled graphene balls with (c) a high-magnification TEM image.

Figure 2. (a) TGA tests of CGO and GO recorded in N_2 at 10 °C/min. The difference in remnant weight was due to pyrolysis of different amounts of oxygenated functional groups. (b) Peak shifting on XRD pattern before and after VAN loaded on CGO suggesting morphological affinity for adsorption. (c) FTIR spectrum demonstrating that CGO maintained oxygenated functional groups after aerosol spray drying and (d) identification of amine groups in CGO−VAN and GO−VAN, confirming the drug complex formation. (e) Water contact angles showing improved wettability of CGO. (f) ζ-Potential validating VAN molecules adsorbed onto the surface of GO or CGO.
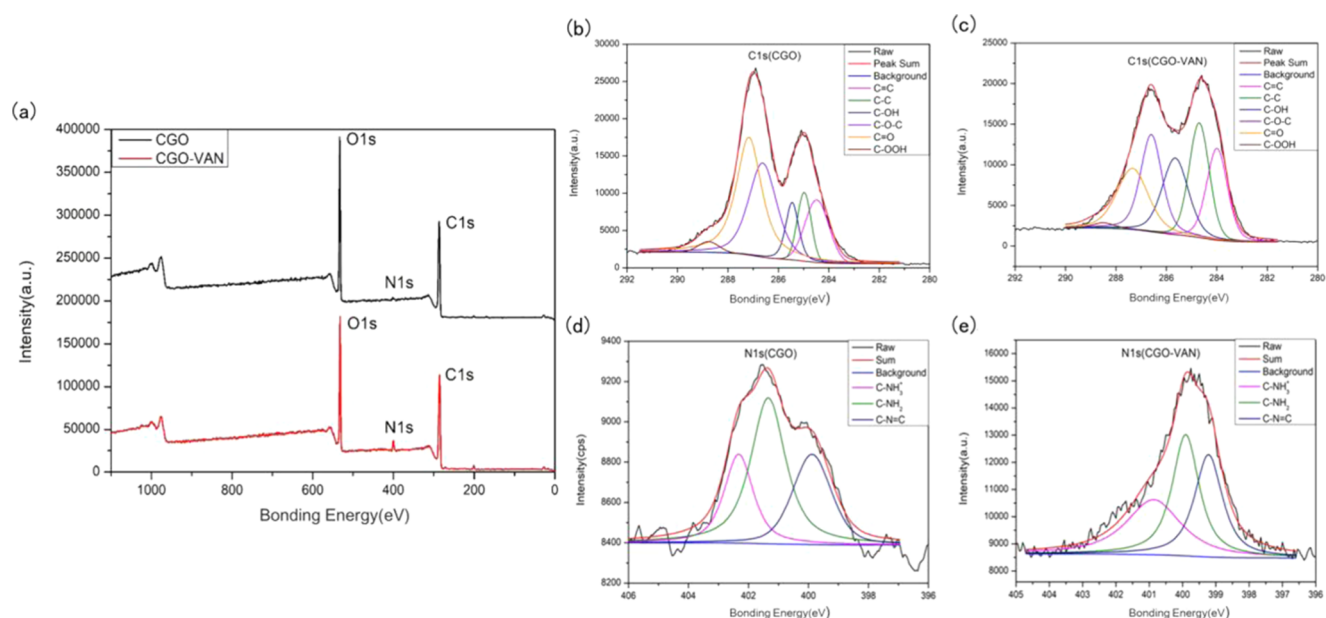
Figure 3. (a) XPS image showing the survey scan of CGO before and after VAN adsorption. (b−e) Detailed XPS scans showing the bonding energies of C 1s and N 1s of CGO before and after VAN adsorption.

flat sheets shown in Figure 1a. CGO was formed through the rapid evaporation of GO aerosol microdroplets, which resulted in a 3D compressed paper ball shape with submicrometer particulate size and rough surface texture shown in Figure 1b. GO microdroplets were prone to dehydration during the process of a passed-through heating zone, and this process could generate confinement force to wrap the planar GO sheets.[23] The detailed structure of CGO under transmission electron microscopy (Figure 1c) shows that the particulate CGO had the intact curvature embedded with channels, which could render the CGO extra free volume for drug adsorption. The intact curvature was inherently derived from completely planar GO sheets and did not significantly reduce the accessible surface area.

The heating treatment during the process of aerosol spray drying would not only cause the shape change of GO but also cause a slight loss of oxygen content.[24] This was revealed from the investigation of thermal stability between GO and CGO in Figure 2a. When the heating temperature approached 100 °C, the adsorbed water in GO and CGO began to release. Because the crumpled and 3D porous structures could provide more free volume for water molecules, CGO lost more weight than GO at around 100 °C. From 200 to 300 °C, the weight loss was due to pyrolysis of oxygenated functional groups.[25] In the same temperature range, CGO lost less weight than GO. This also yielded the final weight remnant difference of 8 wt % between CGO and GO at 800 °C.

The powder X-ray diffraction patterns of the as-prepared GO and CGO displayed a distinguished (001) peak at $2\theta = 11.2°$ (Figure 2b). According to Bragg's law, the intense and narrow peaks of GO were correlated to the 0.80 nm interlayer spacing, which confirmed the presence of oxygenated functional groups on the GO basal sheet since the theoretical interlayer spacing of graphite was 0.34 nm.[26] The weak and broad peaks of CGO at the same diffraction angle reflected the internal stress caused by warped planar GO sheets. After the adsorption of amorphous VAN molecules, diffraction peaks of both GO−VAN ($2\theta = 6.71°$) and CGO−VAN ($2\theta = 9.46°$)

were shifted to the left and became wider compared to those of the as-prepared GO and CGO. This yielded expanded interlayer spacings of 1.32 nm for GO−VAN and 0.93 nm for CGO−VAN as expected due to π−π stacking and hydrogen bonding between carriers and VAN molecules.[27,28] The increments of interlayer spacing after VAN adsorption were 0.52 nm for CGO and 0.13 nm for GO. Apparently, CGO showed reinforced interactions with VAN, which could be accredited to the morphological affinity of the crumpled ball shape for adsorption.

The high presence of the oxygenated groups could demonstrate that CGO had maintained similar chemical functionalities to GO after the aerosol spray drying. According to the Fourier transform infrared spectra in Figure 2c, GO and CGO were offered the same adsorption peaks, such as C=O (1730 cm^{-1}), C−O−C (1168 cm^{-1}), O−H (3426 and 1398 cm^{-1}), and C=C (1626 cm^{-1}) bands.[29] Drug complex formation was confirmed by the appearance of N−H bending (1502 cm^{-1}) and C−N stretching (1224 cm^{-1}) vibrations of amine groups,[30] which was the typical fingerprint group of VAN molecules and not found on the as-prepared CGO and GO (Figure 2d). The identification of amine groups in CGO−VAN and GO−VAN molecules could be contributed to the electrostatic attraction between protonated amine groups from VAN and carboxyl groups on graphene derivatives. In addition, the hydrogen bonding from oxygenated groups and π−π binding from the skeleton of benzene rings, which were both on the surface of graphene derivatives,[31] could also be benefited from the physical adsorption and subsequently delayed the release of VAN.

Both graphene derivatives displayed a net hydrophilicity with terminal carbonyl and carboxyl groups in Figure 2e. The water contact angles between CGO and GO films were 18.63 ± 0.56 and 32.49 ± 0.29°, respectively, and the films dried from solution could display the collective organizational behavior of graphene derivatives on shapes.[32] Therefore, the improved wettability of CGO film was not expected from carboxyl bonds that were hydrophilic in nature[33] but due to
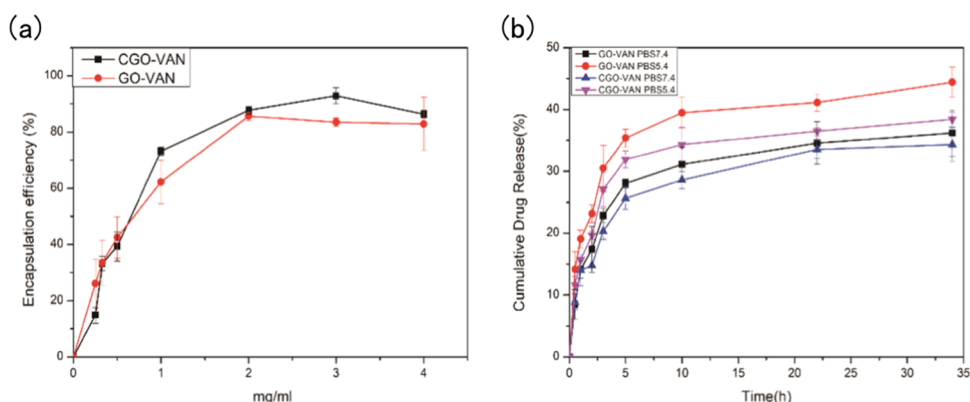
Figure 4. (a) Encapsulation efficiencies of GO−VAN and CGO−VAN drug complexes. (b) pH-responsive release profiles of GO−VAN and CGO−VAN drug complexes.

the presence of crumpled ball shape. The low wetting of CGO film might mean that the water droplet would adequately spread between the liquid and solid interfaces due to attractive capillary force, which arose from wrinkles and ridges in the CGO. The high hydrophilicity of CGO could increase the possibility of interaction with the soluble VAN molecules.

To further understand the surface property and surface charge for the adsorption of VAN, the ζ-potential measurements were carried out for GO, CGO, VAN-loaded GO (GO−VAN), and VAN-loaded CGO (CGO−VAN) systems in Figure 2f. The ζ-potential of CGO was -18.43 ± 0.90 mV and slightly lower than that of GO (-16.95 ± 0.75 mV) in water solution at neutral pH, which should be the result of dissociation of acidic carboxyl groups ($-COOH \leftrightarrow -COO^{-1} + -H^{+1}$).[34] This could assume that the ball-shaped CGO might present the steric repulsion and expose more surface charge positions on the curve and wrinkles of the original basal plane. Since VAN was a potent antibiotic drug-containing cationic group,[35] the positive shifted ζ-potentials after VAN loading were attributed to the electrostatic interaction with the negatively charged surface of the as-prepared GO and CGO. This could validate that VAN molecules were adhered or adsorbed onto the surface of GO sheets or CGO particles. The slightly higher potential of CGO could facilitate the electrostatic attraction of the positively charged VAN and decelerate the drug release afterward compared to GO−VAN.

In addition, VAN adsorption was also revealed from the comparison of chemical analysis through X-ray photoelectron spectroscopy (XPS) measurements of CGO and CGO−VAN samples, as shown in Figure 3. The binding energy peak of N 1s (399 eV)[36] was hardly observed at the survey scan of CGO, whereas the spectra of CGO−VAN were identified as an intensified N 1s peak. This would suggest that the nitrogen-containing groups were complexed with CGO. The N 1s deconvolution spectra of CGO−VAN (Figure 3e) could be fitted to peaks centered at 399.2, 399.9, and 400.9 eV and corresponded to C−N=C, C−NH$_2$, and C−NH$_3^+$ groups,[37] and all three peaks were intensified compared to that in CGO (Figure 3d). These results confirmed that VAN should be functionalized with CGO. The C/O ratio of CGO was 1.88 and the typical C/O ratio of GO was 2,[38] which meant that CGO still kept a large content of oxygen functional groups. The deconvoluted C 1s spectra of CGO−VAN (Figure 3c) were fitted with peaks centered at 284.0, 284.7, 285.7, 286.6, 287.3, and 288.8 eV, which corresponded to C=C, C−C, C−

OH, C−O−C, C=O, and C−OOH.[39] Notably, the intensity of carboxyl group (C−OOH) at CGO decreased after loading VAN, which could be contributed to the preferred electrostatic interaction (amide) between positive amine groups and negative carboxyl groups.

VAN Loading and Release Behavior. VAN as an antibacterial drug was loaded on the GO and CGO carriers via the direct mix-and-rinse method, while unattached VAN was washed out after centrifugation. The encapsulation efficiencies (EEs) of VAN were calculated by measuring the concentration of unattached drug, which was based on relative intensities of UV−vis absorbance. The encapsulation efficiency profiles as a function of GO derivative concentrations in water solution were shown in Figure 4a. At carrier concentrations under 1 mg/mL, the overall presence of GO and CGO was contributed to the accordingly increased VAN loading percentage. For the GO−VAN complexes, the loading capacity approached the highest value of ca. 88% in a 2 mg/mL GO solution and then reached a plateau in GO solution of higher concentrations. Comparably, the VAN loading capacity was higher on CGO than on GO solution from 1 mg/mL, and the maximum loading capacity of CGO was approximately 93% in a 3 mg/mL CGO solution. These EE results were much higher than other carrier materials, such as carbon nanotube[40] and β-tricalcium phosphate beads.[41] The adsorption equilibrium state between VAN and high-concentration GO solution could be considered as a sheetlike surface area that was fully occupied by a branched peptide from VAN molecules. However, the strengthened loading capacity of CGO could be associated with encapsulation within a crumpled ball shape.[42] Additionally, the enlarged hydrophilic and negatively charged surface of CGO could further intensify the attraction of VAN molecules through $\pi-\pi$ stacking.

The in vitro release profiles of VAN from both samples were investigated in phosphate buffer solutions PBS5.4, which represented the inflammation activated by acidic environment, and PBS7.4 for a normal physiological environment. As shown in Figure 4b, VAN was released quickly in the early stages, and this burst release could be beneficial for containing the bacteria.[43] Subsequently, the release rate was gradually declined and these delivery systems were still released after 30 h. The prolonged release was effective to avoid latent infections and counter repeated drug administrations. At basic condition PBS7.4, the release of VAN was slower and reached a lower cumulative quantity from both CGO−VAN and GO−VAN drug complexes compared to that at acidic condition

(PBS5.4). Therefore, CGO−VAN and GO−VAN drug complexes displayed the pH-controlled release property. The cumulative VAN release from CGO−VAN approached around 34.5% in PBS7.4 and 38.4% in PBS5.4 and that from GO−VAN was about 36.2% in PBS7.4 and 41.9% in PBS5.4. This might be due to deprotonation at basic condition that would strengthen the interaction between graphene carriers and VAN through hydrogen bonding. Compared to the GO−VAN system, the VAN was released relatively slowly from the CGO−VAN system in a controlled manner at both PBS5.4 and PBS7.4. Since too much release in the initial stage would cut down the treatment time and cause antibiotic toxicity, the CGO−VAN system would be practical for the delayed drug release. The delayed VAN release from the CGO−VAN system originated from the encapsulation and $\pi-\pi$ stacking of the three-dimensional crumpled ball shape. The robust $\pi-\pi$ stacking between CGO and VAN also resulted in the limited cumulative drug release. In summary, CGO−VAN drug complexes could be potentially applied for deep-seated bacterial infection with high vancomycin loading for pH-responsive release.

CONCLUSIONS

For VAN loading, the maximum encapsulation efficiency of VAN reached 93% when CGO was 3 mg/mL, and 88% when GO was 2 mg/mL. In terms of release, at basic condition, the cumulative VAN release from CGO−VAN was 34.5% and that from GO−VAN was 36.2%. The total released amount of VAN was increased to 38.4% from CGO−VAN and 41.9% from GO−VAN at the acidic condition. The strengthened loading and delayed release of VAN from the CGO−VAN system resulted in the morphological adsorption and encapsulation on the CGO. Nitrogen-containing groups identified on CGO−VAN and GO−VAN drug complexes certified the attachment of VAN on graphene carriers. The improved hydrophilicity and surface charge found on CGO resulted from an intensified $\pi-\pi$ stacking between the crumpled ball shape and VAN. Thus, the crumpled morphology was the main mechanism for the controlled release of VAN from CGO.

EXPERIMENTAL SECTION

Materials. Natural flake graphite with an average particle size of 44 μm, potassium permanganate (KMnO$_4$, AR), and vancomycin hydrochloride (99.95%) were purchased from Aladdin (Shanghai). Sulfuric acid (H$_2$SO$_4$, AR), sodium nitrate (NaNO$_3$, AR), hydrochloric acid (HCl, AR), hydrogen peroxide (H$_2$O$_2$, 30% aq.), and sodium hydroxide (NaOH, AR) were supplied by Sinopharm (Shanghai). Phosphate-buffered saline (PBS) tablets were obtained from BBI Life Sciences (Shanghai). All of the chemicals were used as received without further purification.

Preparation of Graphene Derivatives. Graphene oxide (GO) sheets were prepared through exfoliation of graphite.[44] Briefly, graphite powder (5 g) and NaNO$_3$ (2.5 g) were put into concentrated H$_2$SO$_4$ (115 mL) in an ice bath, and the suspension was stirred for 25 min. Subsequently, KMnO$_4$ (15 g) was added slowly, and the temperature of the suspension was kept below 10 °C for another 25 min. Then, the suspension was heated to 35 °C and kept for 45 min to form a thick paste, which was diluted with deionized water and further reacted at 98 °C. H$_2$O$_2$ was used to neutralize the residual KMnO$_4$. Finally, the mixture was centrifuged and distilled to

reach a pH of 7. The dried GO sample was obtained by freeze-drying the mixture at −60 °C.

Crumpled graphene oxide (CGO) was fabricated through the aerosol spray drying.[23,45] The solution of GO (1 mg/mL) was sprayed through an ultrasonic atomizer to form aerosol droplets, which were carried through a 200 °C quartz tube by 1 L/min N$_2$. GO was conformed to CGO as the water evaporation of aerosol droplets. The CGO particulates were collected from a Teflon filter, which was mounted at the end of the quartz tube.

Fabrication and Testing of VAN-Loaded Drug Systems. The vancomycin (VAN)-loaded GO and CGO drug systems were prepared through the following procedure. VAN was dispersed in water to form 1 mg/mL solution, and GO or CGO particulates were added according to a predetermined weight ratio between carriers and drugs (4:1, 3:1, 2:1, 1:1, 1:2, 1:3, and 1:4). The mixture was homogenized with sonication for 1 h and then magnetically stirred for 24 h at room temperature. The dissociated VAN was removed using extensive centrifugation (12 000 rpm) for 30 min. Afterward, the precipitate was lyophilized to present the GO−VAN or CGO−VAN drug complexes.

The encapsulation efficiencies of drug complexes depended on the attached VAN with GO or CGO divided by the gross weight of VAN in solutions. The attached VAN was decided from the deduction dissociated VAN from the gross weight. The amount of dissociated VAN was quantified using the peak value of UV absorbance at 280 nm,[25] which was substituted into the standard absorbance line equation. The standard absorbance line was built upon the fixed content of VAN solutions, which were 0.1, 0.125, 0.25, 0.5, and 1 mg/mL.

The release behavior of VAN from GO−VAN and CGO−VAN drug complexes was evaluated at two pH values after dialysis.[26,27] The complex (5.0 mg) was placed in a dialysis bag (MWCO MD10), which was immersed in 20 mL of PBS by a pH value of 7.4 (PBS7.4) or 5.4 (PBS5.4). The samples were placed in a shake incubator at 37 °C. At set time points, 50 μL of aliquots were taken from the release medium and the amount of VAN released was monitored by UV−vis spectroscopy. The cumulative drug release was calculated as the amount of VAN released from the drug complex divided by the total mass of VAN in the complex. The average and standard deviations of cumulative drug release were gained after three groups of testing under the same condition at the same time.

General Material Characterization. Fourier transform infrared (FTIR) spectroscopy was carried out on an LAM750 spectrometer (PE Spectrum 100) over the range 4000−400 cm^{-1} and with potassium bromide as the background agent. X-ray diffraction (XRD) was measured using an X-ray diffractometer (Bruker, D8 Advance). The morphology of samples was observed by a field emission scanning electron microscope (FEI, Quanta FEG 450) under 20 kV and a transmission electron microscope (FEI, Tecnai G2) under 200 kV. Water contact angles were measured using a contact angle measurement instrument (CA100C INNUO). Thermogravimetric analysis (TGA) was performed using a thermogravimetric analyzer (TG 209F1, Netzsch Instruments) at a heating rate of 10 °C/min under N$_2$ atmosphere. ζ-Potentials were measured on a Zeta Sizer Nano-ZS90 system (Malvern). UV−vis adsorption spectra were recorded on a UV−vis spectrophotometer (NanoDrop 2000). An X-ray photoelectron spectrometer (Thermo Scientific ESCALAB 250Xi)

equipped with an Al Kα source was used to detect surface chemistry.

■ AUTHOR INFORMATION

Corresponding Authors
*E-mail: hexing@usst.edu.cn (X.H.).
*E-mail: drsujiacan@163.com (J.S.).

ORCID
Jiacan Su: 0000-0001-7080-263X

Author Contributions
∥X.H. and Z.Z. contributed equally to this work.

Notes
The authors declare no competing financial interest.

■ REFERENCES

(1) Murray, B. E.; Arias, C. A.; Nannini, E. C. Mandell, Douglas, and Bennett's Principles and Practice of Infectious Diseases, 8th ed.; Elsevier, 2015; Vol. 1, pp 377−400.

(2) Wang, F.; Zhou, H.; Olademehin, O. P.; Kim, S. J.; Tao, P. Insights into key interactions between vancomycin and bacterial cell wall structures. ACS Omega 2018, 3, 37−45.

(3) Zalavras, C. G.; Patzakis, M. J.; Holtom, P. Local antibiotic therapy in the treatment of open fractures and osteomyelitis. Clin. Orthop. Relat. Res. 2004, 427, 86−93.

(4) Russell, S. L.; Gold, M. J.; Reynolds, L. A.; Willing, B. P.; Dimitriu, P.; Thorson, L.; Redpath, S. A.; Perona-Wright, G.; Blanchet, M.; Mohn, W. W.; Brett Finlay, B.; McNagny, K. M. Perinatal antibiotic-induced shifts in gut microbiota have differential effects on inflammatory lung diseases. J. Allergy Clin. Immunol. Pract. 2015, 135, 100−109.

(5) Shimamoto, Y.; Fukuda, T.; Tanaka, K.; Komori, K.; Sadamitsu, D. Systemic inflammatory response syndrome criteria and vancomycin dose requirement in patients with sepsis. Intensive Care Med. 2013, 39, 1247−1252.

(6) Herzog, T.; Uhl, W. Microbiology for Surgical Infections; Kon, K.; Rai, M., Eds.; Academic Press, 2014; pp 61−76.

(7) Lodise, T. P.; Patel, N.; Lomaestro, B. M.; Rodvold, K. A.; Drusano, G. L. Relationship between initial vancomycin concentration-time profile and nephrotoxicity among hospitalized patients. Clin. Infect. Dis. 2009, 49, 507−514.

(8) Devlin, J. W.; Barletta, J. F. Critical Care Medicine; Mosby, 2008; pp 343−376.

(9) Pelgrift, R. Y.; Friedman, A. J. Nanotechnology as a therapeutic tool to combat microbial resistance. Adv. Drug Delivery Rev. 2013, 65, 1803−1815.

(10) Choi, S. K.; Myc, A.; Silpe, J. E.; Sumit, M.; Wong, P. T.; McCarthy, K.; Desai, A. M.; Thomas, T. P.; Kotlyar, A.; Banaszak Holl, M. M.; Orr, B. G.; Baker, J. R., Jr. Dendrimer-based multivalent vancomycin nanoplatform for targeting the drug-resistant bacterial surface. ACS Nano 2013, 7, 214.

(11) Alenezi, A.; Hulander, M.; Atefyekta, S.; Andersson, M. Development of a photon induced drug-delivery implant coating. Mater. Sci. Eng., C 2019, 98, 619−627.

(12) Pornpattananangkul, D.; Zhang, L.; Olson, S.; Aryal, S.; Obonyo, M.; Vecchio, K.; Huang, C.; Zhang, L. Bacterial toxin-triggered drug release from gold nanoparticle-stabilized liposomes for the treatment of bacterial infection. J. Am. Chem. Soc. 2011, 133, 4132−4139.

(13) Qi, G.; Li, L.; Yu, F.; Wang, H. Vancomycin-modified mesoporous silica nanoparticles for selective recognition and killing of pathogenic gram-positive bacteria over macrophage-like cells. ACS Appl. Mater. Interfaces 2013, 5, 10874−10881.

(14) Kaur, A.; Preet, S.; Kumar, V.; Kumar, R.; Kumar, R. Synergetic effect of vancomycin loaded silver nanoparticles for enhanced antibacterial activity. Colloids Surf., B 2019, 176, 62−69.

(15) Zhou, T.; Zhou, X.; Xing, D. Controlled release of doxorubicin from graphene oxide based charge-reversal nanocarrier. Biomaterials 2014, 35, 4185−4194.

(16) Zhu, S.; Zhen, H.; Li, Y.; Wang, P.; Huang, X.; Shi, P. PEGylated graphene oxide as a nanocarrier for podophyllotoxin. J. Nanopart. Res. 2014, 16, No. 2530.

(17) Xu, L. Q.; Liao, Y. B.; Li, N. N.; Li, Y. J.; Zhang, J. Y.; Wang, Y. B.; Hu, X. F.; Li, C. M. Vancomycin-assisted green synthesis of reduced graphene oxide for antimicrobial applications. J. Colloid Interface Sci. 2018, 514, 733−739.

(18) Weng, W.; Nie, W.; Zhou, Q.; Zhou, X.; Cao, L.; Ji, F.; Cui, J.; He, C.; Su, J. Controlled release of vancomycin from 3D porous graphene-based composites for dual-purpose treatment of infected bone defects. RSC Adv. 2017, 7, 2753−2765.

(19) Esmaeili, A.; Ghobadianpour, S. Vancomycin loaded superparamagnetic MnFe$_2$O$_4$ nanoparticles coated with PEGylated chitosan to enhance antibacterial activity. Int. J. Pharm. 2016, 501, 326−330.

(20) Liu, S.; Hu, M.; Zeng, T. H.; Wu, R.; Jiang, R.; Wei, J.; Wang, L.; Kong, J.; Chen, Y. Lateral dimension-dependent antibacterial activity of graphene oxide sheets. Langmuir 2012, 28, 12364−12372.

(21) Bai, S.; Shen, X.; Zhu, G.; Yuan, A.; Zhang, J.; Ji, Z.; Qiu, D. The influence of wrinkling in reduced graphene oxide on their adsorption and catalytic properties. Carbon 2013, 60, 157−168.

(22) Wang, W. N.; He, X. Aerosol processing of crumpled graphene oxide-based nanocomposites for drug delivery. Curr. Pharm. Des. 2016, 22, 2491−2500.

(23) Luo, J. Y.; Jang, H. D.; Sun, T.; Xiao, L.; He, Z.; Katsoulidis, A. P.; Kanatzidis, M. G.; Gibson, J. M.; Huang, J. X. Compression and aggregation-resistant particles of crumpled soft sheets. ACS Nano 2011, 5, 8943−8949.

(24) El Rouby, W. M. A. Crumpled graphene: preparation and applications. RSC Adv. 2015, 5, 66767.

(25) Sikwal, D. R.; Kalhapure, R. S.; Rambharose, S.; Vepuri, S.; Soliman, M.; Mocktar, C.; Govender, T. Polyelectrolyte complex of vancomycin as a nanoantibiotic: preparation, in vitro and in silico studies. Mater. Sci. Eng., C 2016, 63, 489−498.

(26) Ardeshirzadeh, B.; Anaraki, N. A.; Irani, M.; Rad, L. R.; Shamshiri, S. Controlled release of doxorubicin from electrospun PEO/chitosan/graphene oxide nanocomposite nanofibrous scaffolds. Mater. Sci. Eng., C 2015, 48, 384−390.

(27) Wang, R.; Shou, D.; Lv, O.; Kong, Y.; Deng, L.; Shen, J. pH-controlled drug delivery with hybrid aerogel of chitosan, carboxymethyl cellulose and graphene oxide as the carrier. Int. J. Biol. Macromol. 2017, 103, 248−253.

(28) Zhao, X.; Zou, X.; Ye, L. Controlled pH- and glucose-responsive drug release behavior of cationic chitosan based nanocomposite hydrogels by using graphene oxide as drug nanocarrier. J. Ind. Eng. Chem. 2017, 49, 36−45.

(29) Dong, S.; Xia, L.; Guo, T.; Zhang, F.; Cui, L.; Su, X.; Wang, D.; Guo, W.; Sun, J. Controlled synthesis of flexible graphene aerogels macroscopic monolith as versatile agents for wastewater treatment. Appl. Surf. Sci. 2018, 445, 30−38.

(30) Ma, N.; Liu, J.; He, W.; Li, Z.; Luan, Y.; Song, Y.; Garg, S. Folic acid-grafted bovine serum albumin decorated graphene oxide: An efficient drug carrier for targeted cancer therapy. J. Colloid Interface Sci. 2017, 490, 598−607.

(31) Deng, S.; Berry, V. Wrinkled, rippled and crumpled graphene: An overview of formation mechanism, electronic properties, and applications. Mater. Today 2016, 19, 197−212.

(32) Koltonow, A. R.; Luo, C.; Luo, J.; Huang, J. Graphene oxide sheets in solvents: to crumple or not to crumple? *ACS Omega* **2017**, *2*, 8005−8009.

(33) Rafiee, J.; Rafiee, M. A.; Yu, Z.; Koratkar, N. Superhydrophobic to superhydrophilic wetting control in graphene films. *Adv. Mater.* **2010**, *22*, 2151−2154.

(34) Li, M.; Liu, C.; Xie, Y.; Cao, H.; Zhao, H.; Zhang, Y. The evolution of surface charge on graphene oxide during the reduction and its application in electroanalysis. *Carbon* **2014**, *66*, 302−311.

(35) Seedat, N.; Kalhapure, R. S.; Mocktar, C.; Vepuri, S.; Jadhav, M.; Soliman, M.; Govender, T. Co-encapsulation of multi-lipids and polymers enhances the performance of vancomycin in lipid polymer hybrid nanoparticles: In vitro and in silico studies. *Mater. Sci. Eng., C* **2016**, *61*, 616−630.

(36) Molla, A.; Li, Y.; Mandal, B.; Kang, S. G.; Hur, S. H.; Chung, J. S. Selective adsorption of organic dyes on graphene oxide: theoretical and experimental analysis. *Appl. Surf. Sci.* **2019**, *464*, 170−177.

(37) Ederer, J.; Janos, P.; Ecorchard, P.; Tolasz, J.; Stengl, V.; Benes, H.; Perchacz, M.; Pop-Georgievski, O. Determination of amino groups on functionalized graphene oxide for polyurethane nanomaterials: XPS quantitation vs. functional speciation. *RSC Adv.* **2017**, *7*, 12464−12473.

(38) Kwan, Y. C. G.; Ng, G. M.; Huan, C. H. A. Identification of functional groups and determination of carboxyl formation temperature in graphene oxide using the XPS O 1s spectrum. *Thin Solid Films* **2015**, *590*, 40−48.

(39) Stobinski, L.; Lesiak, B.; Malolepszy, A.; Mazurkiewicz, M.; Mierzwa, B.; Zemek, J.; Jiricek, P.; Bieloshapka, I. Graphene oxide and reduced graphene oxide studied by the XRD, TEM and electron spectroscopy methods. *J. Electron Spectrosc. Relat. Phenom.* **2014**, *195*, 145−154.

(40) Xu, J.; Yudasaka, M.; Kouraba, S.; Sekido, M.; Yamamoto, Y.; Iijima, S. Single wall carbon nanohorn as a drug carrier for controlled release. *Chem. Phys. Lett.* **2008**, *461*, 189−192.

(41) Hess, U.; Mikolajczyk, G.; Treccani, L.; Streckbein, P.; Heiss, C.; Odenbach, S.; Rezwan, K. Multi-loaded ceramic beads/matrix scaffolds obtained by combining ionotropic and freeze gelation for sustained and tuneable vancomycin release. *Mater. Sci. Eng., C* **2016**, *67*, 542−553.

(42) Luo, J.; Zhao, X.; Wu, J.; Dong Jang, H.; Kung, H. H.; Huang, J. Crumpled graphene-encapsulated Si nanoparticles for lithium ion battery anodes. *J. Phys. Chem. Lett.* **2012**, *3*, 1824−1829.

(43) Yu, H.; Yang, P.; Jia, Y.; Zhang, Y.; Ye, Q.; Zeng, S. Regulation of biphasic drug release behavior by graphene oxide in polyvinyl pyrrolidone/poly(ε-caprolactone) core/sheath nanofiber mats. *Colloids Surf., B* **2016**, *146*, 63−69.

(44) Han, Z.; Tang, Z.; Li, P.; Yang, G.; Zheng, Q.; Yang, J. Ammonia solution strengthened three-dimensional macro-porous graphene aerogel. *Nanoscale* **2013**, *5*, 5462−5467.

(45) Tang, Z.; Li, X.; Sun, T.; Shen, S.; Xiu, H.; Yang, J. Porous crumpled graphene with hierarchical pore structure and high surface utilization efficiency for supercapacitor. *Microporous Mesoporous Mater.* **2018**, *272*, 40−43.